MEDICAL IMAGE PROCESSING METHODS FOR THE DEVELOPMENT OF A VIRTUAL ENDOSCOPE

László Szilágyi

Department of Control Engineering and Information Technology
Budapest University of Technology and Economics
H–1117 Budapest, Magyar Tudósok krt. 2, Hungary
e-mail: lazacika@yahoo.com,lalo@ms.sapientia.ro

Abstract

Virtual endoscopes give internal views of the human body without penetrating it, based on a set of parallel cross-sections produced with any computed tomography method. This paper presents some ideas concerning the design and implementation of a software system, which acts like a virtual endoscope. It takes into account the general requirements of the system, gives a solution that uses a multi-step algorithm, and finally shows the resulting 3-D images. Most of the algorithmic steps have several possible solutions. Some comparisons are made among them where appropriate. The quality of service provided by the chosen method mainly depends on the resolution of the input images.

Keywords: virtual reality, endoscope, magnetic resonance imaging, 3-D surface reconstruction

1. Introduction

Traditional endoscopes penetrate the human body in order to provide high-resolution internal views of cavities and hollow organs. Even though such examinations are mostly considered non-invasive, the procedure causes pain, or at least discomforts the patient, who consequently needs some kind of sedation or anaesthesia.

Magnetic resonance imaging (MRI) is a non-invasive diagnostic tool that views the internal anatomy of the human body in 2-D cross sections called slices. A virtual endoscope establishes 3-D internal views based on these sets of 2-D slices, using modern image processing techniques and computer graphics as well. Besides the comfort provided, another relevant advantage is the fact, that it can create images of any body part, not only the hollow ones.

This paper presents a new concept of the virtual endoscope, developed in the Biomedical Engineering Laboratory at TU Budapest. During the development process, MRI brain images are used for testing the methods, but the algorithm is capable to process other kinds of medical images, too. Consequently the virtual endoscope will have several medical applications.

In order to create a virtual endoscope based on magnetic resonance images, the following image processing tasks need to be performed (see *Fig. 1*):

1. filtering the initial MR images,

2. segmentation of the 2-D slices, classification of their pixels into a set of clusters, whose cardinality is set according to the requirements of medical scientists;

3. a shape recovery algorithm is applied to reconstruct the 3-D image of the object;

4. visualization via modern computer graphics tools.
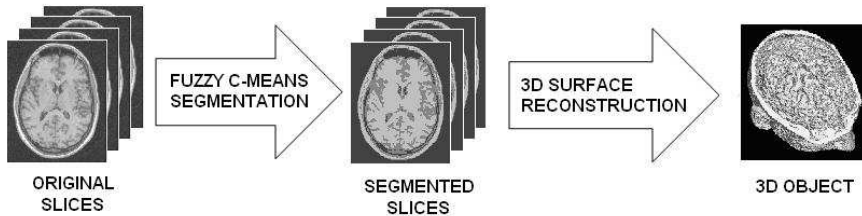
Fig. 1. Main steps of image processing

2. Materials and Methods

2.1. Magnetic Resonance Imaging

Magnetic resonance imaging provides parallel cross sections of the investigated part of the human body. This study is based on a set of 171 slices of the human brain, each of them having 256×256 pixels, thus having a resolution around 1 pixel per mm.

2.2. Filtering Methods

Magnetic resonance images tend to have two main noise types, having several possible sources for each.

High frequency noise manifests as isolated white and black pixels scattered over the whole set of cross sections. They are generally referred to as salt-and-pepper noise. Several implementations use low-pass averaging filtering techniques in order to eliminate these noises [1]. This technique really works fast, it considerably reduces the noise level, but also erects an obstacle to the segmentation as it hides the sharp edges behind an introduced blur. In spite of its slightly higher computational needs, the median filter is a better choice, because it completely eliminates the isolated noisy pixels unless more then 5% of the image pixels are contaminated.

Low frequency noises, often reported as intensity non-uniformities, are caused by the unwanted presence of an intensive bias field that turns some parts of the MR images darker than others. An efficient adaptive estimation method for the distribution of the bias field is presented in [6].

2.3. Segmentation of MRI Brain Slices Using a Modified Fuzzy C-means (FCM) Algorithm

The standard FCM algorithm presented by Bezdek et al. in [3], groups the values x_k, $k = 1..N$ into a number of c clusters, using the objective function

$$J_B = \sum_{i=1}^{c} \sum_{k=1}^{N} u_{ik}^p (x_k - v_i)^2, \tag{1}$$

where v_i represents the prototype value of the ith cluster, u_{ik} represents the fuzzy membership of the kth voxel with respect to cluster i, and p is a weighting exponent. By definition, for any k we have $\sum_{i=1}^{c} u_{ik} = 1$. To minimize the objective function, it is necessary to assign high membership values to those voxels, whose intensities are situated close to the prototype values of their particular clusters.

AHMED et al. proposed a modification to the original objective function by introducing a term that allows the labelling of a voxel to be influenced by the labels in its immediate neighborhood [1]. This effect acts as a regularizer, and biases the solution toward piecewise-homogeneous labelling. The modified objective function is given by

$$J_A = \sum_{i=1}^{c} \sum_{k=1}^{N} \left[u_{ik}^p (x_k - v_i)^2 + \frac{\alpha}{N_k} \sum_{r=1}^{N_k} u_{ik}^p (x_{k,r} - v_i)^2 \right] \tag{2}$$

where $x_{k,r}$ represents the neighbour voxels of x_k, and N_k stands for the number of voxels in the neighbourhood of the kth voxel. The parameter α controls the intensity of the neighbouring effect. This combination of filtering and segmentation made it possible to estimate the contaminating bias field, but considerable reduced its performance against the clock.

In the followings, we will introduce some modifications to this algorithm, in order to reduce its computational needs. It is obvious, that a set of MR brain image slices contains approximately 10^7 voxels. The intensity of the voxels is generally encoded with 8 bit resolution, that is, there are only 256 possible levels of intensity for each voxel. If we perform a median filtering preceding the fuzzy classification, then the formula of this latter does not have to treat each voxel separately. We only need to know, how many voxels of each existing gray level are present in the whole stack of filtered slices. This information is reflected by the histogram. This technique is not applicable using the formulation of [1].

So the proposed enhanced fuzzy C-means algorithm consists of the following steps:

Step 1. First we apply a median filtering to each pixel, using a 3×3 neighbourhood. This means, that the nine intensity values situated in the vicinity of the given pixel are sorted increasingly, and the filtered value will be the one situated in the middle. Let us denote the filtered intensity level of the kth voxel by ξ_k.

Step 2. Let us denote the number of intensity levels by q. As it was previously stated, q is much smaller then N. We denote the number of voxels from the whole stack of filtered slicesby γ_l, having the intensity equal to $\xi_k = l$, where $l = 1..q$ and $k = 1..n$. By definition, we have $\sum_{l=1}^{q} \gamma_l = N$. In the followings, ξ_l will denote the intensity level corresponding to color l.

Step 3. The objective function used for the segmentation of the filtered image will be:

$$J_S = \sum_{i=1}^{c} \sum_{l=1}^{q} \gamma_l u_{il}^{p} (\xi_l - v_i)^2. \tag{3}$$

We need to find those values of the parameters u_{il} and v_i, for which this objective function has the minimal value. Let us consider the Lagrange multiplier

$$F_S = \sum_{i=1}^{c} \sum_{l=1}^{q} \left[\gamma_l u_{il}^{p} (\xi_l - v_i)^2 \right] + \sum_{l=1}^{q} \lambda_l \left(1 - \sum_{i=1}^{c} u_{il} \right). \tag{4}$$

Step 4. Taking the derivative of F_S with respect to u_{il}, and equalling it to 0, we get:

$$\frac{\delta F_S}{\delta u_{il}} = p\gamma_l u_{il}^{p-1} (\xi_l - v_i)^2 - \lambda_l = 0, \text{ so } u_{il} = \left(\frac{\lambda_l}{p\gamma_l} \right)^{\frac{1}{p-1}} (\xi_l - v_i)^{\frac{-2}{p-1}}. \tag{5}$$

From $\sum_{j=1}^{c} u_{jl} = 1$, we obtain

$$\lambda_l = p\gamma_l \left[\sum_{j=1}^{c} (\xi_l - v_j)^{\frac{-2}{p-1}} \right]^{1-p}, \text{ and so } u_{il} = \left[\sum_{j=1}^{c} \left(\frac{\xi_l - v_i}{\xi_l - v_j} \right)^{\frac{2}{p-1}} \right]^{-1}. \tag{6}$$

Step 5. Taking the derivative of F_S with respect to v_i, and equalling it to 0, we get:

$$\frac{\delta F_S}{\delta v_i} = -2 \cdot \sum_{l=1}^{q} \left(\gamma_l u_{il}^{p} (\xi_l - v_i) \right) = 0, \text{ so } v_i = \left(\sum_{l=1}^{q} \gamma_l u_{il}^{p} \xi_l \right) \left(\sum_{l=1}^{q} \gamma_l u_{il}^{p} \right)^{-1}. \tag{7}$$

The proposed modified FCM algorithm for 2-D segmentation is summarized in *Fig. 2*.

Attempts for further development of the standard FCM algorithm, in the direction of local and adaptive processing, are presented in [2] and [11].
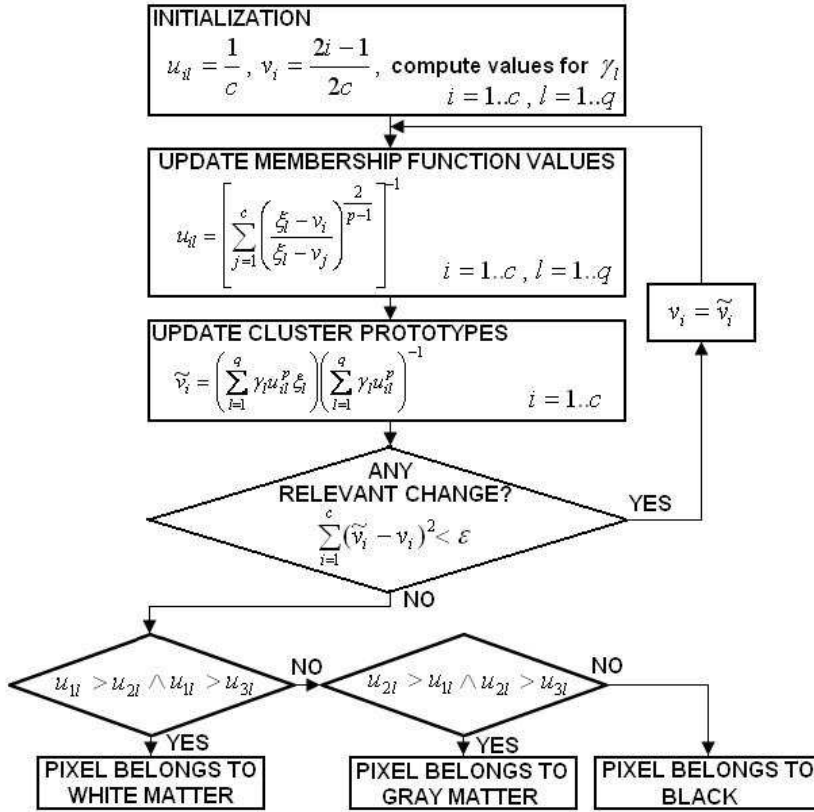
Fig. 2. Schematic representation of the modified fuzzy classification algorithm

2.4. 3-D Surface Reconstruction Methods

Three dimensional shape recovery is the key problem of this whole image processing tool. A traditional and widely used solution is to apply the marching cube algorithm, because it is easily understandable and gives acceptable results. Alternative experiments use elastic surfaces to estimate the 3-D shape of the investigated objects. All these methods rely on the results and side-products of the 2-D segmentation.

Any voxel k in the investigated volume ($k = 1..N$) has a probability of belonging to the 3-D region named class i equal to the fuzzy membership function value u_{ik}. Based on these values, we can define the region indicator scalar spaces R_i, having the value at voxel k given by the formula $R_{ik} = 1 - 2u_{ik}$. The region indicator will be negative inside the region, positive outside the region, and the boundary surface of the region will be the zero level set of this scalar space.

2.4.1. The Marching Cube Algorithm

The marching cube algorithm divides the whole investigated volume into unitary sized cubes, having at its corners 2×2 adjacent pixels of two neighbouring slices. Based on the region indicator values of these 8 voxels, it determines whether the zero level set intersects this cube and if so, it also locates the intersection. As any of the 8 voxels can be either inside or outside the 3-D region we wish to detect, there are $2^8 = 256$ different cases. Symmetry assigns these cases to 14 different topologies, which are shown in *Fig. 3*. Voxels inside the region are represented with black circles, while white circles show the voxels situated outside [7]. The obtained surface elements unambiguously define the 3-D boundary surface of the region only if we decide a priori, which regions will be treated with 6-connectivity.
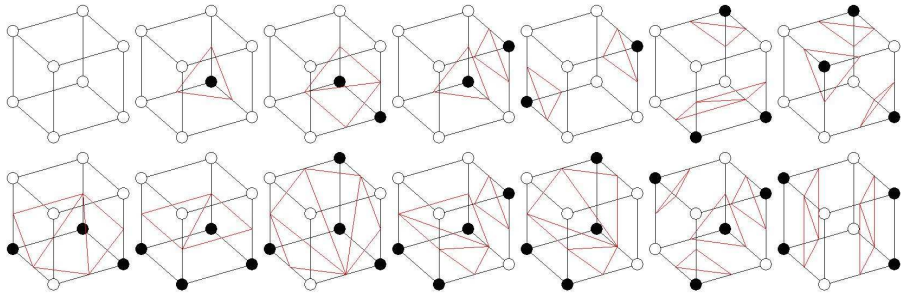
Fig. 3. The fourteen different topologies of the marching cube algorithm

The surface elements compose a high-resolution 3-D view with a considerable accuracy. That is why even nowadays several medical imaging systems are being developed using this concept.

2.4.2. Elastic Surfaces

The zero level set of the region indicator R_i is the ideal surface boundary of the 3-D region classified in class i. Our task is to define a propagating closed surface within the region and then to make this surface approximate the zero level set as accurate as possible. The accuracy will mainly depend on the gradient values around the zero level, because sharper edges are easier to localize. A stopping force is needed so that the propagating surface stops at the appropriate place.

Gradient-driven stopping force was introduced by CASELLES et al [4] and MALLADI et al [9]. Their solution had a significant weakness with the pulling back feature, that is, when a front crossed the aim boundary, it could not come back. To avoid this problem, YEZZI et al [17] and KICHENASSAMY et al [5] introduced their additional stopping force term due to edge strength. To improve the boundary leak characteristics, SIDDIQUI et al [12] added another extra stopping term due to

area minimization. The most recent advance in the domain is the usage of curvature dependent stopping forces introduced by LORIGO et al [8] and MALLADI et al [10].

The complete summary of elastic-surface-based 3-D shape recovery methods is presented in [13].

2.5. *Visualization Issues*

Visualization issues generally refer to development tasks. In our case an OpenGL-based user interface is needed, which provides interactivity facilities in order to perform the virtual penetration, and instantly shows the internal view of the investigated organ.

3. Results and Discussion

3.1. *Filtering*

The median filter vs. averaging low-pass filter has significant advantages, namely:

1. it acts less sensitively to severe contamination with salt-and-pepper noise;
2. it does not blur the sharp edges;
3. it also has a shape regularizer effect.

3.2. *Fuzzy Segmentation*

Due to medical requirements, the brain images are generally segmented in three classes: white matter, gray matter, and black. The fuzzy C-means classification performs a quick convergence. *Fig. 4* shows, that the number of necessary cycles mainly depends on the initialization of cluster prototypes, but the resulting proto-types values do not vary. So the initial values of cluster prototypes may be random values with the constraint that they differ from each other [14, 15]. *Fig. 5* presents the obtained fuzzy membership functions.

Fig. 6 uses three brain cross sections to show the result of the fuzzy clustering. On the left side we can see an original MR brain slice, in the middle the output of the median filter is presented, while the one on the right side is the output of the fuzzy segmentation. *Fig. 7* shows a cross section of the region indicator scalar spaces corresponding to the white matter and gray matter [16].
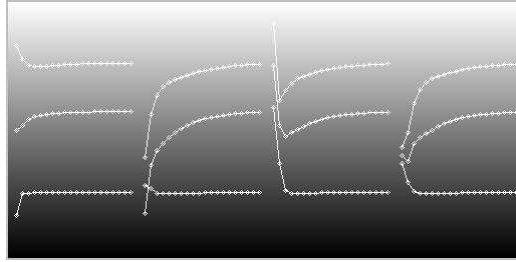
Fig. 4. Converging cluster prototypes with different initializations
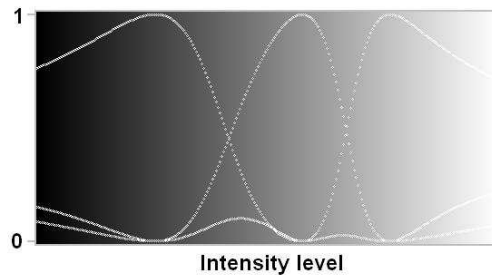
Fig. 5. The fuzzy membership functions of the three clusters
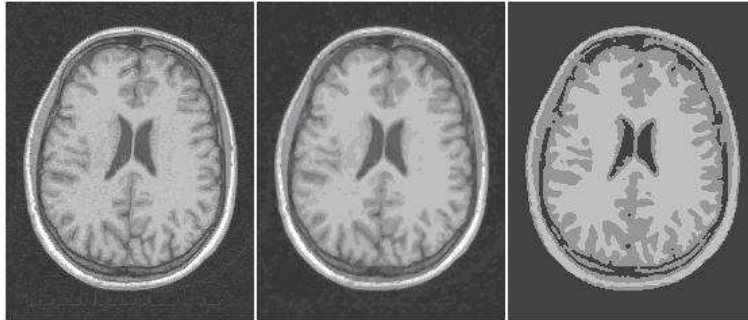
Fig. 6. MR brain cross sections: original (left), after preprocessing with median filter (middle), segmented using the proposed version of FCM (right)

3.3. 3-D Surface Reconstruction

Fig. 8 shows a 3-D endoscopic view of the cortical surface, reconstructed using the described methods. The clarity and sharpness of the view, and the smoothness of the obtained shape are excellent reasons for acceptance.
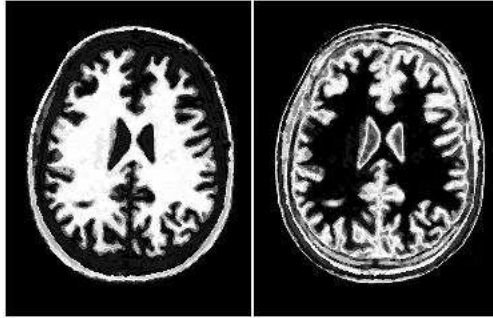
Fig. 7. Intensity plots of white (left) and gray matter (right) probabilities
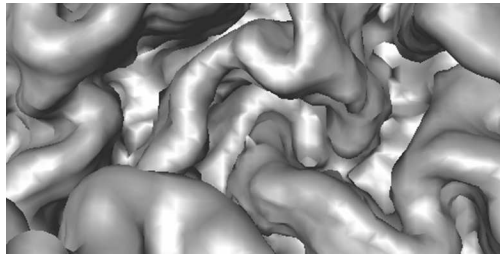
Fig. 8. 3-D endoscopic view obtained using the proposed algorithms

4. Conclusions

The proposed algorithms provide fast image processing and lead to smooth boundaries between the black, gray, and white matter. The obtained 3-D image still has to improve, but results are promising. In order to visualize smaller details of the human body with the right accuracy, higher-resolution MR images will be needed. The presented algorithms are capable to support a virtual brain endoscope.

Acknowledgements

References

[1] AHMED, M. N.– YAMANY, S. M. – MOHAMED, N.– FARAG, A. A.– MORIARTY, T.: A Modified Fuzzy C-Means Algorithm for Bias Field Estimation and Segmentation of MRI Data, *IEEE Trans. Medical Imaging*, **21/3** (2002), pp. 193–199.

[2] ARDEKANI, S. – KANGARLOO, H. – SINHA, U.: Region Based Fuzzy Clustering for Automated Brain Segmentation, *Proc. 2nd Joint IEEE EMBS/BMES Conference, Houston*, 2002, pp. 1041–1042.

[3] BEZDEK, J. C.– HALL, L.–CLARKE, L.: Review of MR image segmentation using pattern recognition, *Med. Phys.*, **20** (1993), pp. 1033-1048.

[4] CASELLES, V. – CATTE, F. – COLL, T. – DIBOS, F.: A Geometric Model for Active Contours, *Numer. Math.*, **66/1** (1993), pp. 1–31.

[5] KICHENASSAMY, S. – KUMAR, A. – OLVER, P.– TANNENBAUM, A. – YEZZI, A.: Conformal curvatures flows: From phase transitions to active vision, *Arch. Rational Mech. Anal.*, **134/3** (1996), pp. 275–301.

[6] LIEW, A. W. C. – YAN, H.: An Adaptive Spatial Fuzzy Clustering Algorithm for 3-D MR Image Segmentation, *IEEE Trans. Medical Imaging*, Vol. 22, No. 9, pp. 1063-1075, 2003.

[7] LORENSEN, W. E.– CLINE, H. E.: Marching Cubes: a High Resolution 3D Surface Construction Algorithm, *Computer Graphics*, **21/ 4** (1987), pp. 163-169.

[8] LORIGO, L. M.– GRIMSON, W. – ERIC, L. – FAUGERAS, O.– KERIVEN, R.– KIKINIS, R.– NABAVI, A.– WESTIN, C. F.: Two Geodesic Active Contours for the Segmentation of Tubular Structures, *Proc. Comput. Vision Pattern Recognition*, June 2000, pp. 444–451.

[9] MALLADI, R. – SETHIAN, J. A. – VEMURI, B. C.: Shape Modeling with front Propagation, *IEEE Trans. Pattern Anal. Machine Intell.*, **17/2** (1995), pp. 158–175.

[10] MALLADI, R. – SETHIAN, J. A.: An O(N log N) Algorithm for Shape Modeling, *Appl. Math., Proc. Nat. Academy Sci.*, **93/18** (1996), pp. 9389–9392.

[11] PHAM, D. L.– PRINCE, J. L.: Adaptive Fuzzy Segmentation of Magnetic Resonance Images, *IEEE Trans. Medical Imaging*, **18/9** (1999), pp. 737–752.

[12] SIDDIQUI, K.– LAURIERE, Y. B.– TANNENBAUM, A.– ZUCKER, S. W.: Area and Length Minimizing Flows for Shape Segmentation, *IEEE Trans. Image Processing*, **7** (1998), pp. 433–443.

[13] SURI, J. S. – LIU, K.– SINGH, S.– LAXIMINARAYAN, S.– ZENG, X.– REDEN, L.: Shape Recovery Algorithms Using Level Sets in 2-D/3-D Medical Imagery: A State-of-the-Art Review, *IEEE Trans. Information Technology in Biomedicine,* **6/1** (2002), pp. 8–28.

[14] SZILÁGYI, L.– BENYÓ, Z: Magnetic Resonance Brain Image Segmentation Using an Enhanced Fuzzy C-Means Algorithm, Proc. WC2003 World Congress on Medical Physics and Biomedical Engineering, Sydney, 2003, paper #4406, pp. 1–4.

[15] SZILÁGYI, L.: Virtual Brain Endoscopy Based on Magnetic Resonance Images, *Periodica Politechnica, TU Timisoara, Trans. Automatic Control and Computer Science*, **49/63** (2004), pp. 47-50.

[16] SZILÁGYI, L.– SZILÁGYI, S. M. – BENYÓ, Z.: Medical Image Segmentation for Virtual Endoscopy, *Proc. 16th IFAC World Congress*, 2005, Prague, paper#1775, pp. 1–5.

[17] YEZZI, A.-KICHENASSAMY, S.– KUMAR, A.– OLVER, P.– TANNENBAUM, A.: A Geometric Snake Model for Segmentation of Medical Imagery, *IEEE Trans. Medical Imaging*, **16** (1997), pp. 199–209.